Current Applied Physics xxx (2017) 1–6

Contents lists available at ScienceDirect

Current Applied Physics

journal homepage: www.elsevier.com/locate/cap

Enhanced and broadband absorber with surface pattern design for X-Band

Chenguang Wu [a, b, c], Shuwen Chen [b, c], Xisheng Gu [b, c], Renchao Hu [b, c], Shuomin Zhong [d], Guoguo Tan [b, c, *], Qikui Man [b, c, **], Chuntao Chang [b, c], Xinmin Wang [b, c], Run-Wei Li [b, c]

[a] Nano Science and Technology Institute, University of Science and Technology of China, Suzhou, Jiangsu 215123, China
[b] Key Laboratory of Magnetic Materials and Devices, Ningbo Institute of Materials Technology & Engineering, Chinese Academy of Sciences, Ningbo, Zhejiang 315201, China
[c] Zhejiang Province Key Laboratory of Magnetic Materials and Application Technology, Ningbo Institute of Materials Technology & Engineering, Chinese Academy of Sciences, Ningbo, Zhejiang 315201, China
[d] Faculty of Electrical Engineering and Computer Science, Ningbo University, Ningbo, Zhejiang 315211, China

ARTICLE INFO

Article history:
Received 19 April 2017
Received in revised form
12 October 2017
Accepted 17 October 2017
Available online xxx

Keywords:
Microwave absorber
Surface pattern design
Broadband
Carbonyl iron

ABSTRACT

A broadband and thin-layer microwave absorber is designed based on surface pattern design made by carbonyl iron and rubber composite. The bandwidth with reflection less than −10 dB covers the full X-band owing to two absorption peaks appeared simultaneously in both the simulation results and experimental results. In this work, the power loss and power flow diagram were present by CST simulation, which clearly explain the broadband absorption caused by double λ/4 matching absorption and interfacial scattering synergistic effect. A facile splicing method was provided to extend the absorption bandwidth for the magnetic absorbing materials.

Contents

1. Introduction

Microwave absorbing materials (MAMs) have wide applications in civilian and modern military areas such as electromagnetic interference (EMI) protection, antenna and electromagnetic wave stealth [1–5]. Broad absorption bandwidth is critical to evaluate MAMs since electromagnetic device and military radar work in a wide frequency range [6].

Generally, the microwave absorption performance depends on its complex permittivity ($\varepsilon_r = \varepsilon' - j\varepsilon''$), complex permeability ($\mu_r = \mu' - j\mu''$), sample thickness and frequency range [7]. However,

* Corresponding author. Key Laboratory of Magnetic Materials and Devices, Ningbo Institute of Materials Technology and Engineering, Chinese Academy of Sciences, No. 1219 Zhongguan West Road, Zhenhai District, Ningbo 315201, PR China.
** Corresponding author. Key Laboratory of Magnetic Materials and Devices, Ningbo Institute of Materials Technology and Engineering, Chinese Academy of Sciences, No. 1219 Zhongguan West Road, Zhenhai District, Ningbo 315201, PR China.
E-mail addresses: kant01@126.com (G. Tan), manqk@nimte.ac.cn (Q. Man).

https://doi.org/10.1016/j.cap.2017.10.012
1567-1739/

suffering from the Snoek's limit [8,9], it is difficult to further increase the permeability for magnetic material in higher frequency. Hence, the loss mechanisms such as magnetoelectric control [10,11], multiple reflections effect [12,13] or resonance absorption [14,15] are inevitable to broaden the magnetic materials absorption bandwidth. Wan et al. [16] synthesized FeCo-coated carbon fibers to regulate permeability for magnetoelectric control, the permittivity and the permeability can be well matched at high frequencies, the absorption bandwidth of reflection loss (RL) below −10 dB is about 2.5 GHz with absorber thicknesses of 1.3–1.5 mm. Furthermore, the multiple reflections of electromagnetic waves in the absorber are also used to design broadband absorbing material. Due to the extension of electromagnetic waves' propagation path, the power loss of electromagnetic waves can be effectively increased. The bandwidth of natural microcrystalline graphite/low density polyethylene (MG/LDPE) composites with RL less than −10 dB reaches 3.02 GHz at the thickness of 2.0–2.1 mm [7]. Taking advantage of the emerging concept of metamaterials, Li et al. [17] provided an ultra-broadband microwave hybrid absorber, which shows 90% absorption over 2–18 GHz with the effective thickness of 21 mm. However, broadband absorbing materials designed by above methods are either not wide enough or hard to mold, which greatly restricts the applications in practice.

In this work, a facile splicing method was proposed to design a broadband and thin-layer microwave absorber in order to overcome the problem of narrow absorption bandwidth for single λ/4 matching absorption due to the thickness sensitivity. The designed parameters are optimized using a frequency domain solver, implemented by CST MWS. The broadband microwave absorber was fabricated and RL was measured. The RL below −10 dB covers the whole X-band and the experimental results agree well with the simulation results. Finally, broadband characteristics and loss mechanisms of the absorber were discussed in details.

2. Simulation methods and experiments

The broadband absorption properties of the former designed MAM are demonstrated by numerical simulations using a commercial finite-element-method (FEM) by CST MWS simulation software. Based on waveguide as the perfect conductor, ideal electricity boundary is set around the MAMs. The size of the absorbing material was determined by the port size of standard X-band waveguide, and the sketch map of waveguide and the absorber were shown in Fig. 1(a) and (b), respectively.

The carbonyl iron particles (CIs) were uniformly dispersed in the mixed rubber with a volume percentage of 35%, and the mixed rubber was composed of styrene-butadiene rubber (SBR) and PU by mass ratio of 3:1. CIs, SBR and PU were mixed directly (Cyclohexanone was used to solvent), then the mixture was taken uniformly under ultrasonic stirring for 8 h, and absorbing film was obtained by tape casting method. Finally, the absorber with a stepped structure was obtained by hot pressing method.

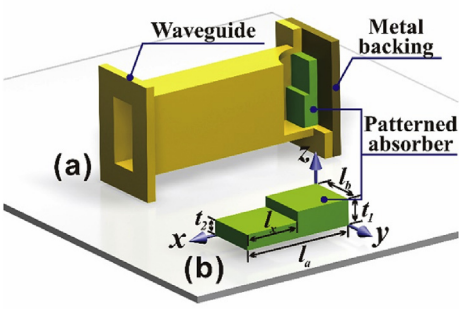

Fig. 1. (a) Schematic 3D view of the patterned absorber in X-band waveguide for simulation and measurement. (b) Enlarged view of the absorber with l_a = 22.8 mm, l_b = 10.1 mm, t_1 = 2.1 mm and t_2 = 1.7 mm.

The phase was examined by X-ray diffraction (XRD, Bruker AXS) using Cu-Kα radiation. The morphology was analyzed by scanning electron microscope (SEM, Hitachi S-4800). The complex permeability of these composite samples were obtained by using an Agilent N5225A vector network analyzer in the 0.1–18 GHz.

3. Results and discussion

The phase and morphologies of CIs were observed by XRD and SEM, respectively. Fig. 2(a) shows the diffraction pattern for CIs which has three narrow peaks at 44.7°, 65.0° and 82.3° corresponding to (110), (200), and (211) of α-Fe, respectively. The integrated characterizations of the as-obtained typical spherical CIs as shown in Fig. 2(b), and the quantitative analysis (inset Figure) presents the diameter of the CI particles, which measured on average 0.9 μm, ranges from 0.1 to 3 μm.

Fig. 3(a) gives the complex permittivity ($\varepsilon_r = \varepsilon' - j\varepsilon''$) and complex permeability ($\mu_r = \mu' - j\mu''$) values of the CI/rubber composite at frequency range of 0.1–18 GHz, including their real part and imaginary part. The permittivity is almost consent in the entire frequency range, and the permeability imaginary part (μ'') has a rising trend after 1 GHz. As a comparison between complex permittivity and complex permeability in the entire measurement range, though ε_r is larger than μ_r, the magnetic loss tangent ($\tan\delta_m = \mu''/\mu'$) is larger than the dielectric loss tangent ($\tan\delta_e = e''/e'$), which explains that CI is a typical magnetic loss material, as shown in Fig. 3(b).

In order to characterize the electromagnetic wave absorption performance of the single-layer CI/rubber composite, the RL curves at different absorber thickness are calculated by using Eqs. (1) and (2) according to transmission-line theory [18].

$$Z_{in} = Z_0\sqrt{\frac{\mu_r}{\varepsilon_r}}\tanh\left[j\left(\frac{2\pi ft}{c}\right)\sqrt{\mu_r\varepsilon_r}\right] \quad (1)$$

$$RL(dB) = 20\lg\left|\frac{Z_{in} - Z_0}{Z_{in} + Z_0}\right| \quad (2)$$

Where Z_{in} represents impedance of the composite, Z_0 is intrinsic impedance of free space, μ_r and ε_r are the complex permeability and complex permittivity. f represents frequency, t represents the absorber thickness, c represents velocity of light in free space. Fig. 4 shows the frequency dependence of RL of the CI/rubber composite samples at three different thicknesses. It can be found that the absorption peak moves to lower frequency with the increase of thickness, and the absorption peak frequency and intensity strongly depends on the absorber thickness. The λ/4 cancelation theory has been frequently employed to explain this phenomenon [19,20]. Here, the bandwidth is defined as the frequency width in which the absorption is less than −10 dB. When the thickness is 1.9 mm, the bandwidth is the widest. However, it is worth noting that the absorber with a thickness of 1.9 mm has RL values exceeding −10 dB in the 8.3–11.7 GHz range, as well as the bandwidth below −15 dB is only 1.8 GHz.

The patterned absorber is designed and fabricated as a stepped structure as shown in Fig. 1(b). The patterned absorber consists of two units with sizes of l_x × 10.1 mm × 1.7 mm, (22.8 mm−l_x) × 10.1 mm × 2.1 mm, respectively. By changing the value of l_x, the relationship between l_x and the bandwidth of MAMs can be gained, as shown in Fig. 5. The bandwidth with RL < −10 dB

Please cite this article in press as: C. Wu, et al., Enhanced and broadband absorber with surface pattern design for X-Band, Current Applied Physics (2017), https://doi.org/10.1016/j.cap.2017.10.012

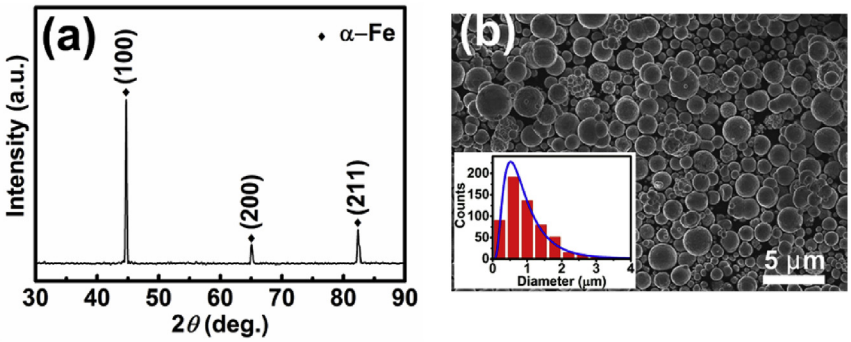

Fig. 2. XRD spectrum (a) of the CIs and (b) representative SEM image corresponding to powers. Inset shows a quantitative analysis of their diameter distribution.

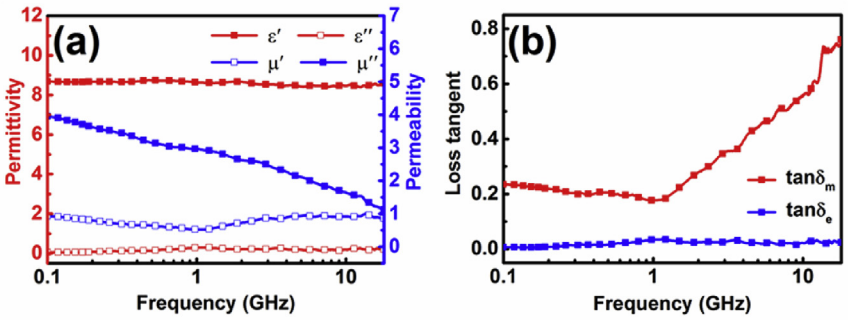

Fig. 3. Frequency dependence of the complex permeability (μ_r), permittivity (ε_r) (a) and loss tangent (b) of CI/rubber composite with 35 vol%.

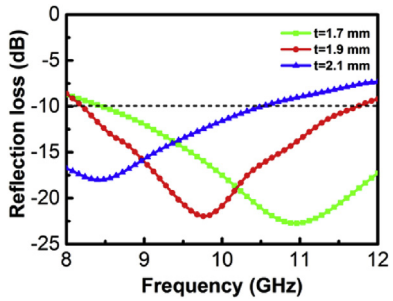

Fig. 4. RL curves for CI/rubber composite with 35 vol% at thickness of 1.7 mm, 1.9 mm and 2.1 mm, respectively.

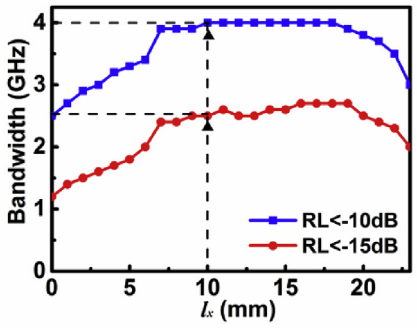

Fig. 5. Dependence of bandwidth on l_x at the fixed t_1 and t_2 for patterned absorber with RL < − 10 dB and RL < − 15 dB, respectively.

and RL < −15 dB almost synchronization changes during the increase of l_x. The bandwidth with RL < −10 dB increased as the l_x increases from a to 10 mm. When l_x gets to 10 mm, the bandwidth of the absorbing materials with RL below −10 dB covered the whole X-band, and the bandwidth with RL < −15 dB arrived 2.5 GHz simultaneously. The black triangle represents the minimum value of l_x that satisfied the optimization condition at the same time.

Fig. 6(a) presents the RL curves for the patterned microwave absorber, and the corresponding percentage absorption is shown in Fig. 6(b). The results indicate that the experimental values are almost identical to the simulation ones. The rationality of simulation method is directly approved. It has been widely reported to use metamaterial absorber for enhancing bandwidth. For example, Ghosh et al. [21] presented a bandwidth-enhanced dual-layer dual-band metamaterial absorber, which occurred three and five distinct absorption peaks in C band and X band, respectively. Bhattacharyya et al. [22] proposed an ultrathin polarization-insensitive structure, which exhibits a broadband of 0.33 GHz above 85% absorption with two absorption peaks. Compared with the above researches, two strong absorption peaks appeared in X band simultaneously, which greatly broadens the absorption band. If the effects brought by the stepped structure are ignored and only considering the absorber as simple combination of two flat absorbers, the resulted reflection can be calculated by sum of the two RL value weighted through their corresponding areas. Thus, the total absorption can be calculated by the following formula [6].

$$RL_{sum}(dB) = 10\lg\sum_{i} S_i \times 10^{RL_i(dB)/10} \quad (3)$$

where S_i represents area fraction of subunit i, RL_i represents reflection loss of subunit i. The calculated result is plotted in Fig. 6(a) as a black curve, which weighted by their areas in the patterned absorber according to Eq. (3). It indicates that the percentage absorption of calculation result is about 5%–10% lower than the experimental and simulated values, which means certain

Please cite this article in press as: C. Wu, et al., Enhanced and broadband absorber with surface pattern design for X-Band, Current Applied Physics (2017), https://doi.org/10.1016/j.cap.2017.10.012

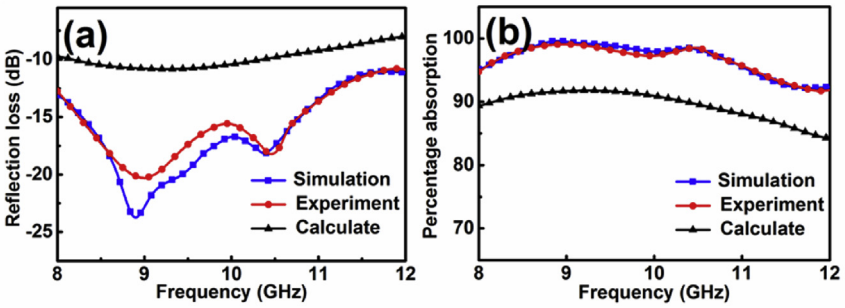

Fig. 6. Reflection loss (a) and percentage absorption (b) for patterned absorber at the fixed l_x. The curves of experimental and simulation were obtained by a standard X-band rectangular waveguide and CST MWS, respectively. The black curve shows the sum reflection loss.

loss mechanism were introduced by combination of the two-flat certain. Thus, although the extra loss value is slight compared with the overall absorption, the absorber performance of the broadband absorber did further improved.

In order to explore the mechanisms for appearing two absorption peaks of the pattern absorber, normalized power loss was calculated, as shown in Fig. 7(a). Results illustrate that the normalized power loss shows two distinct absorption peaks as well as a slight one marked as red and black star, which is consistent with the simulation curve, as shown in Fig. 6. What's more, it could be found that the peak frequencies of stepped shape absorber have a bit offset relative to single layers, which could be understood roughly that equivalent thicknesses were changed. To further study, power loss distribution map of patterned absorber corresponding to 8.5 GHz,8.9 GHz, 10.4 GHz and 10.9 GHz were selected, respectively. 8.5 GHz and 10.9 GHz correspond to the matching frequencies under thickness of 1.7 mm and 2.1 mm for the single layer absorbing film. Meanwhile normalization processing of the power loss was carried out with the maximum power loss value. As shown in Fig. 7(b) and (e), it is apparently to see that the maximum power loss occurs at thickness of 2.1 mm in low frequency (8.5 GHz). With the increasing of frequencies, the maximum loss value moves to the region corresponding to the thin layer and it is in agreement with the observations in former single layer absorbing films, as shown in Fig. 4. According to the λ/4 cancelation theory

$$t_m = \frac{c}{4f_m\sqrt{|\mu_r\varepsilon_r|}} \tag{4}$$

where t_m and f_m are matching thickness and matching frequency, respectively. The matching thickness is reduced gradually with the increase of frequency at the given μ_r and ε_r. This phenomenon is in accordance with our observation. That is to say that patterned absorber occurred twice λ/4 matching absorption in the X-band. Fig. 7(c) and (d) show the power loss corresponding to 8.9 GHz and 10.4 GHz, respectively. Electromagnetic wave is strongly absorbed both in thin layer and thick layer under the frequency of 8.9 GHz, while the power loss under 10.4 GHz is similar to the loss under 10.9 GHz. It is also reflected in the RL curve shown in Fig. 6(a), where the RL has a minimum value under the 8.9 GHz. What's more, there is a strong electromagnetic wave absorption area under those four different frequencies, as a result to the patterned absorber obtains a good absorption in full X-band. The reason for the above phenomenon is probably the stage, which generated in the process of two subunits linear combination. On the other hand, the absorption of matching layer near the step reduced a little. Nevertheless, the absorption of the mismatch thickness enhanced at the same time. It is very beneficial to improve absorption bandwidth.

To further investigate the contribution of the step in the process of electromagnetic wave transmission, power flow distributions at four fixed frequencies were analyzed, as shown in Fig. 8. The red dotted line frame (x: 11–15 mm, z: 1–2.5 mm) in Fig. 7(b) represents selection area. The directions and magnitudes of power flows on the planes in the four different frequencies are also marked using arrows. The patterned absorber provides a redundant step, which could diffract the incident electromagnetic wave. However, if the diffraction effect exists, and then the diffracted microwaves transmitted into the absorber, there will be a change of the power flow direction. It is revealed that in the stepped structure absorber, the power flow obliquely from the corners and side boundaries into the absorber, which indirect evidence that the step has taken place in electromagnetic wave diffraction, and thus enhance the overall absorption. Then the contribution of the step to the power loss was given, the influence area and the absorption performance of the area was showed roughly. The mutations areas of the electromagnetic wave were determined by those points in which their power loss changes greatly during transmission. The mutations areas of

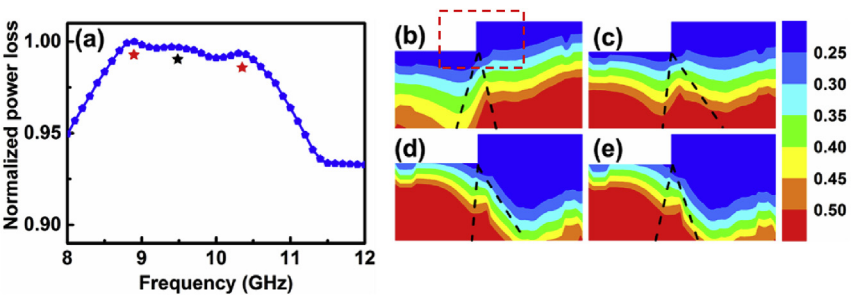

Fig. 7. (a) Normalized power loss of patterned absorber was shown in X-band. Power loss distribution map at fixed frequencies on xz cross-section: (b) 8.5 GHz, (c) 8.9 GHz, (d) 10.4 GHz and (e) 10.9 GHz.

Please cite this article in press as: C. Wu, et al., Enhanced and broadband absorber with surface pattern design for X-Band, Current Applied Physics (2017), https://doi.org/10.1016/j.cap.2017.10.012

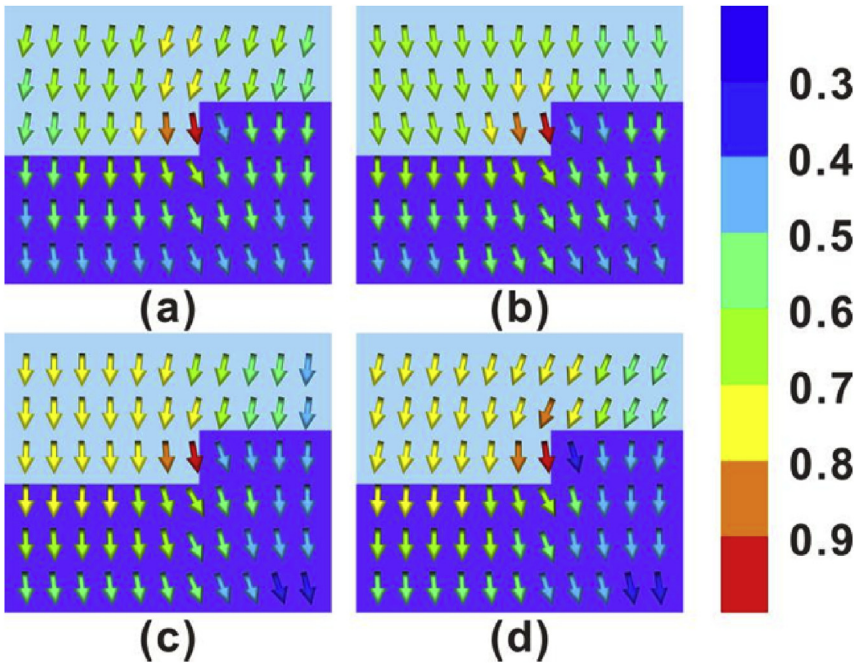

Fig. 8. Power flow distribution map of patterned absorber corresponding to fixed frequency: (a) 8.5 GHz, (b) 8.9 GHz, (c) 10.4 GHz and (d) 10.9 GHz. The selection area was represented by a red dotted line frame (x:11–15 mm, z:1–2.5 mm) in Fig. 7(b). (For interpretation of the references to colour in this figure legend, the reader is referred to the web version of this article.)

the electromagnetic wave were marked with black dashed line, as shown in Fig. 7(b)–(e), respectively. The area of the region and loss percentage were calculated. Results shown that the affected area accounting for a total area is about 8%–14%, corresponding the loss in the area accounts for 10%–16% of overall, the loss percent of dotted box is always greater than the area percent. The existence of the step strengthens the overall absorption but the effect is not obvious. It is consistent with result in Fig. 6(b), that although simulation results and experimental results are also greater than calculation results, the latter only has 5%–8% less, compared to the former. In general, absorbing performance is mainly depend on the double λ/4 matching absorption of the stepped shape absorbing material.

4. Conclusions

A broadband and thin-layer microwave absorber is designed and experimentally realized, based on a facile splicing method. CST software simulation optimization greatly simplifies the complex design process. RL value of the stepped shape patterned absorber below −10 dB covered the whole X-band, and bandwidth of RL below −15 dB is about 2.5 GHz (8.2–10.7 GHz), which has a significant promotion, compared with monolayer absorber. The patterned absorber appeared twice λ/4 matching absorption in the X-band through two different thicknesses. The simulation shows that electromagnetic wave diffraction occurs in the steps, which enhances the overall absorption further. This surface pattern design method provides us a new approach to build broadband absorber, which may have potentials in high performance microwave absorber design.

Acknowledgments

This work was supported by the National Natural Science Foundation of China (Grant No.51301189), Zhejiang Province Public Technology Research and Industrial Projects (Grant No.2015C31043), Ningbo International Cooperation Projects (Grant No. 2015D10022), and the National Key Research and Development Program of China, (Grant No. 2016YFB0300501).

References

[1] H.A. Reshi, A.P. Singh, S. Pillai, R.S. Yadav, S.K. Dhawan, V. Shelke, Nanostructured $La_{0.7}Sr_{0.3}MnO_3$compounds for effective electromagnetic interference shielding in the X-band frequency range, J. Mater. Chem. C 3 (2015) 820–827.
[2] X.L. Dong, X.F. Zhang, H. Huang, F. Zuo, Enhanced microwave absorption in Ni/polyaniline nanocomposites by dual dielectric relaxations, Appl. Phys. Lett. 92 (2008), 013127.
[3] X. Li, X. Guo, T. Liu, X. Zheng, J. Bai, Shape-controlled synthesis of Fe nanostructures and their enhanced microwave absorption properties at L-band, Mater. Res. Bull. 59 (2014) 137–141.
[4] I. Choi, J.G. Kim, I.S. Seo, D.G. Lee, Radar absorbing sandwich construction composed of CNT, PMI foam and carbon/epoxy composite, Compos. Struct. 94 (2012) 3002–3008.
[5] W. Li, C. Le, J. Lv, W. Huang, L. Qiao, J. Zheng, et al., Electromagnetic and oxidation resistance properties of core-shell structure flaked carbonyl iron powder@SiO2 nanocomposite, Phys. Status Solidi A 214 (2017), 1600747.
[6] W. Li, T. Wu, W. Wang, P. Zhai, J. Guan, Broadband patterned magnetic microwave absorber, J. Appl. Phys. 116 (2014), 044110.
[7] W. Xie, X. Zhu, S. Yi, J. Kuang, H. Cheng, W. Tang, et al., Electromagnetic absorption properties of natural microcrystalline graphite, Mater. Des. 90 (2016) 38–46.
[8] G.G. Bush, Generalization of Snoek's limit for modeling initial permeability of magnetic materials, J. Appl. Phys. 63 (1988) 3765–3767.
[9] O. Acher, S. Dubourg, Generalization of Snoek's law to ferromagnetic films and composites, Phys. Rev. B 77 (2008).
[10] X. Zhao, Z. Zhang, L. Wang, K. Xi, Q. Cao, D. Wang, et al., Excellent microwave absorption property of Graphene-coated Fe nanocomposites, Sci. Rep. 3 (2013) 3421.
[11] X.G. Liu, D.Y. Geng, Z.D. Zhang, Microwave-absorption properties of FeCo microspheres self-assembled by Al_2O_3-coated FeCo nanocapsules, Appl. Phys. Lett. 92 (2008), 243110.
[12] A. Wang, W. Wang, C. Long, W. Li, J. Guan, H. Gu, et al., Facile preparation, formation mechanism and microwave absorption properties of porous carbonyl iron flakes, J. Mater. Chem. C 2 (2014) 3769–3776.
[13] C. Wei, X. Shen, F. Song, Y. Zhu, Y. Wang, Double-layer microwave absorber based on nanocrystalline $Zn_{0.5}Ni_{0.5}Fe_2O_4$/α-Fe microfibers, Mater. Des. 35 (2012) 363–368.
[14] W. Li, J. Wei, W. Wang, D. Hu, Y. Li, J. Guan, Ferrite-based metamaterial microwave absorber with absorption frequency magnetically tunable in a wide

range, Mater. Des. 110 (2016) 27–34.
[15] Y. Luo, H.X. Peng, F.X. Qin, M. Ipatov, V. Zhukova, A. Zhukov, et al., Fe-based ferromagnetic microwires enabled meta-composites, Appl. Phys. Lett. 103 (2013) 251902.
[16] Y. Wan, J. Xiao, C. Li, G. Xiong, R. Guo, L. Li, et al., Microwave absorption properties of FeCo-coated carbon fibers with varying morphologies, J. Magn. Magn. Mater. 399 (2016) 252–259.
[17] W. Li, T. Wu, W. Wang, J. Guan, P. Zhai, Integrating non-planar metamaterials with magnetic absorbing materials to yield ultra-broadband microwave hybrid absorbers, Appl. Phys. Lett. 104 (2014), 022903.
[18] J.R. Liu, M. Itoh, K.-I. Machida, Electromagnetic wave absorption properties of α-Fe/Fe_3B/Y_2O_3 nanocomposites in gigahertz range, Appl. Phys. Lett. 83 (2003) 4017–4019.
[19] S.L. Wen, Y. Liu, X.C. Zhao, J.W. Cheng, H. Li, Synthesis, dual-nonlinear magnetic resonance and microwave absorption properties of nanosheet hierarchical cobalt particles, Phys. Chem. Chem. Phys. 16 (2014) 18333–18340.
[20] Y. Yong, Y. Yang, X. Wen, D. Jun, Microwave electromagnetic and absorption properties of magnetite hollow nanostructures, J. Appl. Phys. 115 (2014) 17A521.
[21] B. Somak, G. Saptarshi, C. Devkinandan, V.S. Kumar, Bandwidth-enhanced dual-band dual-layer polarization-independent ultra-thin metamaterial absorber, Appl. Phys. A 118 (2014) 207–215.
[22] G. Saptarshi, B. Somak, V.S. Kumar, Bandwidth-enhancement of an ultrathin polarization insensitive metamaterial absorber, Microw. Opt. Technol. Lett. 56 (2014) 350–355.

Please cite this article in press as: C. Wu, et al., Enhanced and broadband absorber with surface pattern design for X-Band, Current Applied Physics (2017), https://doi.org/10.1016/j.cap.2017.10.012